nature physics

SUPPLEMENTARY INFORMATION

https://doi.org/10.1038/s41567-018-0072-5

In the format provided by the authors and unedited.

Multiscale unfolding of real networks by geometric renormalization

Guillermo García-Pérez[1,2], Marián Boguñá[1,2] and M. Ángeles Serrano[1,2,3]*

[1]Departament de Física de la Matèria Condensada, Universitat de Barcelona, Barcelona, Spain. [2]Universitat de Barcelona Institute of Complex Systems (UBICS), Universitat de Barcelona, Barcelona, Spain. [3]ICREA, Barcelona, Spain. *e-mail: marian.serrano@ub.edu

Supplementary Information for "Multiscale unfolding of real complex networks by geometric renormalization"

Guillermo García-Pérez,[1,2] Marián Boguñá,[1,2] and M. Ángeles Serrano[1,2,3]

[1] *Departament de Física de la Matèria Condensada, Universitat de Barcelona, Martí i Franquès 1, 08028 Barcelona, Spain*
[2] *Universitat de Barcelona Institute of Complex Systems (UBICS), Universitat de Barcelona, Barcelona, Spain*
[3] *ICREA, Pg. Lluís Companys 23, E-08010 Barcelona, Spain*

Contents

I. EVIDENCE OF GEOMETRIC SCALING IN REAL NETWORKS

The real networks analyzed in this paper are:

- The Internet at the Autonomous Systems level. The data was collected by the Cooperative Association for Internet Data Analysis (CAIDA) [1] and corresponds to mid 2009.
- The Airports network. It was obtained from Ref. [2, 3]. Directed links represent flights by airlines. We consider the undirected version obtained by keeping bidirectional edges only.
- The one-mode projection onto metabolites of the human metabolic network at the cell level, as used in Ref. [4].
- The human HI-II-14 interactome. This proteome network was obtained from Ref. [5]. We removed self-loops.
- The Music network. Nodes are chords—sets of musical notes played in a single beat—and connections represent observed transitions among them in a set of songs, see Ref. [6]. The original network is weighted, directed and very dense. Hence, we applied the disparity filter [7] with $\alpha = 0.01$ to obtain a sparser network. Finally, we kept bidirectional edges only to construct the undirected network.
- The Words network is the network of adjacency between words in Darwin's book "The Origin of Species", from Ref. [8].
- The network of email communication within the Enron company was obtained from Refs. [9, 10].
- The Drosophila network is a functional connectome within the Drosophila melanogaster optic medulla related to the motion detection circuit, from Ref. [11].

In all cases, we only considered the largest connected components. Table S1 contains their main topological features.

Name	**Type**	**Nodes**	N	γ	β	$\langle k \rangle$	$\langle c \rangle$
Internet	Technological	Autonomous systems	23748	2.17	1.44	4.92	0.61
Metabolic	Bio/Cell	Metabolites	1436	2.6	1.3	6.57	0.54
Music	Language	Chords	2476	2.27	1.1	16.66	0.82
Airports	Transportation	World airports	3397	1.88	1.7	11.32	0.63
Proteome	Bio/Cell	Proteins	4100	2.25	1.001	6.52	0.09
Words	Language	Words	7377	2.25	1.01	11.99	0.47
Enron	Social/Email	Employees	33696	2.66	1.2	10.73	0.70
Drosophila	Bio/Connectome	Neurons	1770	1.91	1.125	10.01	0.34

TABLE S1: **Overview of the considered real-world networks.** Topological details of the datasets used.

Fig. 2 in the main paper compares the topological properties of the renormalized networks for three real networks. We show the equivalent results for the Airports, Proteome, Words, Enron and Drosophila networks in Fig. S1.

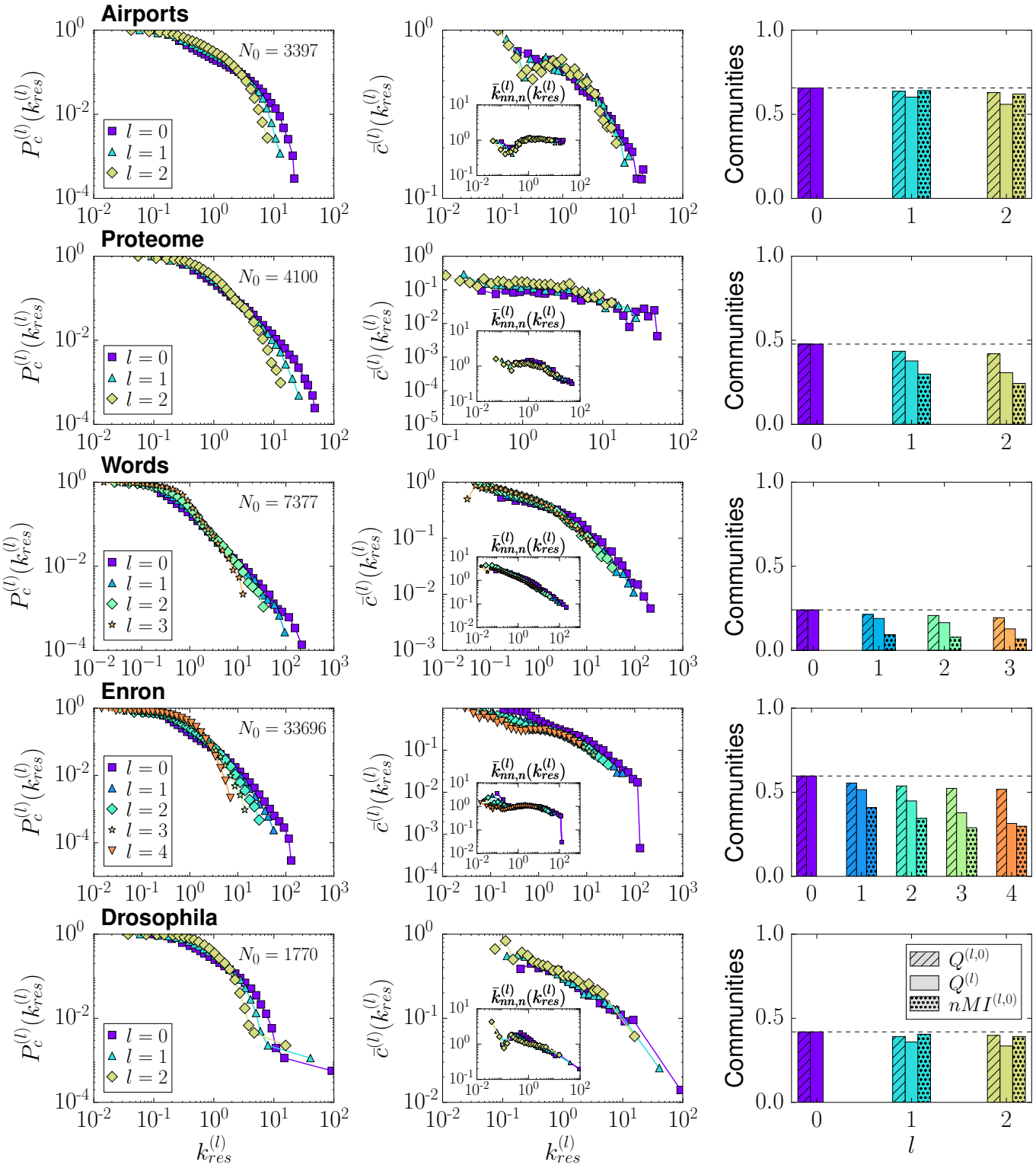

FIG. S1: **Self-similarity along the RGN flow.** Each row shows the RGN flows of different topological features of the Airports, Proteome, Words, Enron and Drosophila networks with $r = 2$. **Left:** Complementary cumulative distribution of rescaled degrees $k_{res}^{(l)} = k^{(l)}/\langle k^{(l)}\rangle$. **Middle:** Local clustering averaged over rescaled-degree classes. The insets show the normalized average nearest neighbour degree $\bar{k}_{nn,n}(k_{res}^{(l)}) = \bar{k}_{nn}(k_{res}^{(l)})\langle k^{(l)}\rangle/\langle (k^{(l)})^2\rangle$. **Right:** RGN flow of the community structure; $Q^{(l)}$ stands for the modularities in every layer l, $Q^{(l,0)}$ is the modularity that the community structure in the l layer induces in the original network, and $nMI^{(l,0)}$ is the normalized mutual information between both partitions. The number of layers in each system is determined by their original size.

In Fig. S2, we show the empirical connection probabilities of the eight real-world networks considered in this paper as well as their renormalized versions.

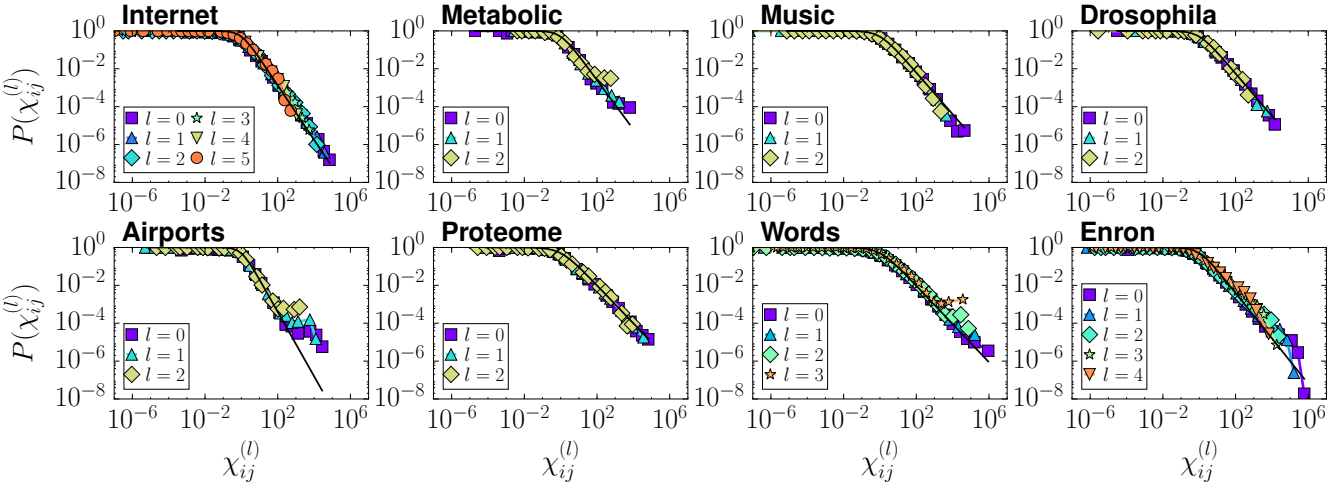

FIG. S2: **Empirical connection probabilities.** Fraction of connected pairs within a given range of $\chi_{ij}^{(l)}$ for the eight real-world networks and their renormalized versions. The black curve is the theoretic connection probability.

II. THE GEOMETRIC RENORMALIZATION GROUP

This section contains the calculations related to the theoretical aspects of the geometric renormalization transformation presented in the main paper. In particular, we show the semigroup structure of the transformation, derive the corresponding recurrence relations for the renormalization of the $\mathbb{S}^1$ model and calculate the flow of the average degree. We also discuss the connection with statistical mechanics by using the isomorphism between the $\mathbb{S}^1$ and the $\mathbb{H}^2$ models and, finally, we include some numerical results regarding the relation between global properties of the networks generated by the model and the flow of the average degree.

A. The semigroup structure of the coarse-graining step

It is easy to show that the geometric coarse-graining presented in the paper has the semigroup structure. To this end, we need to see that node i is mapped to the same supernode whether we apply the coarse-graining with $r = r_1$ first and then a second time with $r = r_2$ or just once with $r = r_1 r_2$. In the first case, the step with $r = r_1$ maps i to supernode $m = \lfloor i/r_1 \rfloor$ (where $\lfloor x \rfloor$ represents the integer part of x), and then m is mapped to $n = \lfloor m/r_2 \rfloor = \lfloor \lfloor i/r_1 \rfloor /r_2 \rfloor$ in the second step. In the second case, i is mapped to supernode $s = \lfloor i/(r_1 r_2) \rfloor$. Notice that $s = \lfloor (i/r_1)/r_2 \rfloor = \lfloor (\lfloor i/r_1 \rfloor + \alpha)/r_2 \rfloor = \lfloor (m+\alpha)/r_2 \rfloor$, where $\alpha = (i \mod r_1)/r_1 < 1$. Now,

$$\frac{m+\alpha}{r_2} = \frac{m}{r_2} + \frac{\alpha}{r_2} = \left\lfloor \frac{m}{r_2} \right\rfloor + \frac{m \mod r_2}{r_2} + \frac{\alpha}{r_2}, \tag{S1}$$

so

$$\left\lfloor \frac{m+\alpha}{r_2} \right\rfloor = \left\lfloor \frac{m}{r_2} \right\rfloor \Leftrightarrow \frac{m \mod r_2}{r_2} + \frac{\alpha}{r_2} < 1, \tag{S2}$$

which is always fulfilled since $\alpha < 1$ and

$$\frac{m \mod r_2 + \alpha}{r_2} \leq \frac{r_2 - 1 + \alpha}{r_2} = 1 + \frac{\alpha - 1}{r_2} < 1. \tag{S3}$$

Thus, $s = n$, and node i is mapped to the same supernode in both cases. It follows immediately from this result that both processes yield the same final link structure.

B. Selecting long-range connections

As we apply the renormalization transformation, some links are integrated inside the supernodes, so they do not contribute to the topology of the renormalized network. In Fig. S3, we show that links joining nodes separated a large angular distance $\Delta\theta_{ij}$ require larger values of r to be integrated; in other words, the connections in a renormalized network represent long-range connections in the original graph.

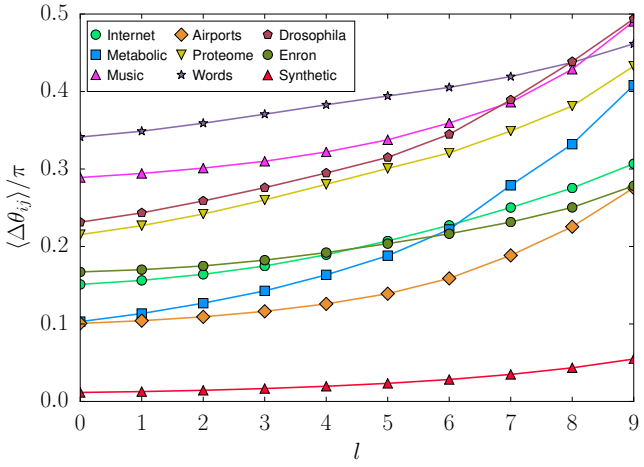

FIG. S3: **Connection range in renormalized layers.** Normalized angular distance $\langle\Delta\theta_{ij}\rangle$ averaged over all links that are not integrated inside a supernode in layer l with $r = 2$.

C. Geometric renormalization of the $\mathbf{S}^1$ model

In this subsection, we derive the RG equations of the $\mathbb{S}^1$ model. In order to simplify the notation, all unprimed quantities will refer to layer $l-1$, whereas primed ones will correspond to layer l. Moreover, we consider the particular case in which all supernodes contain the same number of nodes (r) for simplicity, although the following calculations are also valid for supernodes of different sizes.

Consider the probability p'_{ij} for two supernodes i and j in layer l to be connected, which is given by the probability for at least one link between a pair of the nodes within the supernodes in layer $l-1$ to exist,

$$p'_{ij} = 1 - \prod_{e=1}^{r^2} (1 - p_e)\,, \tag{S4}$$

where e runs over all pairs of nodes (m, n) with m in supernode i and n in supernode j. The term p_e is the probability for m and n to be connected in layer $l-1$,

$$p_e = \frac{1}{1 + \left(\frac{R\Delta\theta_e}{\mu(\kappa_m\kappa_n)_e}\right)^{\beta}}. \tag{S5}$$

Eq. (S4) takes the same functional form as Eq. (S5),

$$p'_{ij} = 1 - \prod_{e=1}^{r^2} \frac{1}{1 + \left(\frac{R\Delta\theta_e}{\mu(\kappa_m\kappa_n)_e}\right)^{-\beta}} = 1 - \frac{1}{\prod_{e=1}^{r^2} 1 + \left(\frac{\mu(\kappa_m\kappa_n)_e}{R\Delta\theta_e}\right)^{\beta}} = 1 - \frac{1}{1+\Phi'_{ij}} = \frac{1}{1+\frac{1}{\Phi'_{ij}}} \tag{S6}$$

with

$$\Phi'_{ij} = \sum_{e=1}^{r^2} \left(\frac{\mu(\kappa_m\kappa_n)_e}{R\Delta\theta_e}\right)^{\beta} + \sum_{e=1}^{r^2-1} \sum_{f=e+1}^{r^2} \left(\frac{\mu(\kappa_m\kappa_n)_e}{R\Delta\theta_e}\right)^{\beta} \left(\frac{\mu(\kappa_m\kappa_n)_f}{R\Delta\theta_f}\right)^{\beta} + \dots \tag{S7}$$

Since the angular distance between the nodes inside each block is generally smaller than the distance between i and j, all the $\Delta\theta_e$ are approximately equal ($\Delta\theta_e \approx \Delta\theta$), so we can write

$$\Phi'_{ij} \approx \left(\frac{\mu}{R\Delta\theta}\right)^{\beta} \sum_{e=1}^{r^2} (\kappa_m\kappa_n)_e^{\beta} + \left(\frac{\mu}{R\Delta\theta}\right)^{2\beta} \sum_{e=1}^{r^2-1} \sum_{f=e+1}^{r^2} (\kappa_m\kappa_n)_e^{\beta} (\kappa_m\kappa_n)_f^{\beta} + \dots \tag{S8}$$

The $\mathbb{S}^1$ model assumes a uniform density of nodes $\delta = 1$, which means that $R = \frac{N}{2\pi}$, whereas μ is a constant independent of N. Indeed, $\frac{\mu}{R} \ll 1$, so the first term leads Eq. (S8) in most cases. Thus,

$$\Phi'_{ij} \approx \left(\frac{\mu}{R\Delta\theta}\right)^{\beta} \sum_{e=1}^{r^2} (\kappa_m\kappa_n)_e^{\beta}. \tag{S9}$$

Introducing this result into Eq. (S6),

$$p'_{ij} \approx \frac{1}{1 + \left(\frac{R\Delta\theta}{\mu}\right)^{\beta} \frac{1}{\sum_{e=1}^{r^2} (\kappa_m\kappa_n)_e^{\beta}}}, \tag{S10}$$

we see that, in order for the resulting expression to be congruent with the model, we need a set of equations that transform the parameters according to

$$\left(\frac{R\Delta\theta}{\mu}\right)^{\beta} \frac{1}{\sum_{e=1}^{r^2} (\kappa_m\kappa_n)_e^{\beta}} = \left(\frac{R'\Delta\theta'_{ij}}{\mu'\kappa'_i\kappa'_j}\right)^{\beta'}. \tag{S11}$$

Let us now assume that the angular coordinate of a supernode is some generalised center of mass of the nodes it integrates, so the separation between the two renormalised nodes $\Delta\theta'_{ij}$ is approximately equal to the angular separation between the nodes that belong to different blocks, i.e. $\Delta\theta'_{ij} \approx \Delta\theta$; thus, $\beta' = \beta$. The choice $\delta = 1$ leads to $R' = \frac{R}{r}$, that is, to the rescaling step. Setting $\mu' = \frac{\mu}{r}$, Eq. (S11) further requires

$$\left(\kappa'_i\kappa'_j\right)^{\beta} = \sum_{e=1}^{r^2} (\kappa_m\kappa_n)_e^{\beta}, \tag{S12}$$

which is fulfilled if

$$\kappa'_i = \left(\sum_{j=1}^{r} \kappa_j^{\beta}\right)^{1/\beta}. \tag{S13}$$

The transformation of masses preserves the semigroup structure exactly, since

$$(\kappa''_i)_r = \left(\sum_{j=1}^{r} \left(\kappa'_j\right)^{\beta}\right)^{1/\beta} = \left(\sum_{j=1}^{r}\sum_{k=1}^{r} \kappa_{j,k}^{\beta}\right)^{1/\beta} = (\kappa'_i)_{r^2}\,. \tag{S14}$$

We should require the transformation of angles to preserve it as well. This can be achieved using the following generalised center of mass

$$\theta'_i = \left(\frac{\sum_{j=1}^{r} (\theta_j\kappa_j)^{\beta}}{\sum_{j=1}^{r} \kappa_j^{\beta}}\right)^{1/\beta}, \tag{S15}$$

given that

$$(\theta''_i)_r = \frac{1}{(\kappa''_i)_r} \left(\sum_{j=1}^{r} \left(\theta'_j\kappa'_j\right)^{\beta}\right)^{1/\beta} = \frac{1}{(\kappa'_i)_{r^2}} \left(\sum_{j=1}^{r} \left(\kappa'_j\right)^{\beta} \frac{1}{\left(\kappa'_j\right)^{\beta}} \sum_{k=1}^{r} (\theta_{j,k}\kappa_{j,k})^{\beta}\right)^{1/\beta} = (\theta'_i)_{r^2}\,. \tag{S16}$$

D. RG flow of the average degree

As discussed in the previous subsection, as we renormalize, we move in the space of realizations of the $\mathbb{S}^1$ model, always keeping the congruency between the network and the hidden metric space, i.e. Eq. (S5). Therefore, we can use the $\mathbb{S}^1$ model to compute the average degree $\langle k' \rangle$ of the renormalised networks. According to Ref. [12],

$$\langle k' \rangle = C_0 \mu' \langle \kappa' \rangle^2, \tag{S17}$$

where C_0 does not change as we renormalize. We thus need to compute $\langle \kappa' \rangle$, where κ' is given by Eq. (S13) and the original distribution of masses is assumed to be a power-law,

$$\rho(\kappa) = \frac{1-\gamma}{\kappa_c^{1-\gamma} - \kappa_0^{1-\gamma}} \kappa^{-\gamma}, \quad \kappa \in [\kappa_0, \kappa_c]. \tag{S18}$$

The strategy to compute $\langle \kappa' \rangle$ is as follows: **1.** We define $z \equiv \kappa^\beta$ and find their distribution $\rho_z(z)$. **2.** We then calculate $\hat{\rho}_z^r(s)$ (where $\hat{\rho}_z(s)$ is the Laplace transform of $\rho_z(z)$); according to the convolution theorem, this is the Laplace transform of the variable $z' \equiv \sum_r z = \kappa'^\beta$. **3.** Finally, we compute $\langle \kappa' \rangle$ as the $1/\beta$-th moment of z', that is, $\langle \kappa' \rangle = \langle z'^{1/\beta} \rangle$, from $\hat{\rho}_z^r(s)$.

1. From Eq. (S18),

$$\rho(\kappa)\mathrm{d}k = \frac{1-\gamma}{\kappa_c^{1-\gamma} - \kappa_0^{1-\gamma}} \kappa^{-\gamma} \mathrm{d}\kappa = \frac{1-\gamma}{\beta \left(\kappa_c^{1-\gamma} - \kappa_0^{1-\gamma} \right)} z^{\frac{1-\gamma}{\beta} - 1} \mathrm{d}z, \tag{S19}$$

so

$$\rho_z(z) = \frac{1-\gamma}{\beta \left(\kappa_c^{1-\gamma} - \kappa_0^{1-\gamma} \right)} z^{-\eta}, \tag{S20}$$

where $\eta = \frac{\gamma - 1}{\beta} + 1$.

2. If $\gamma < 2\beta + 1$, $\eta < 3$, which means that z' and, consequently, κ' are also power-law distributed since the central limit theorem does not apply (the opposite case corresponds to phase III in Fig. 3**C** in the paper) [13]. The Laplace transform of Eq. (S20) is given by

$$\hat{\rho}_z(s) = \int_{\kappa_0^\beta}^{\kappa_c^\beta} \rho_z(z) e^{-sz} \mathrm{d}z = \frac{(1-\gamma) \left(\Gamma(1-\eta, s\kappa_0^\beta) - \Gamma(1-\eta, s\kappa_c^\beta) \right)}{\beta \left(\kappa_c^{1-\gamma} - \kappa_0^{1-\gamma} \right)} s^{\eta - 1}, \tag{S21}$$

where $\Gamma(a, b)$ is the incomplete gamma function,

$$\Gamma(a, b) = \int_b^\infty t^{a-1} e^{-t} \mathrm{d}t. \tag{S22}$$

From this result, it follows that

$$\hat{\rho}_{z'}(s) = \left[\frac{(1-\gamma) \left(\Gamma(1-\eta, s\kappa_0^\beta) - \Gamma(1-\eta, s\kappa_c^\beta) \right)}{\beta \left(\kappa_c^{1-\gamma} - \kappa_0^{1-\gamma} \right)} s^{\eta - 1} \right]^r. \tag{S23}$$

3. We need to compute

$$\langle z'^{1/\beta} \rangle = \int_0^\infty z'^{1/\beta} \rho_{z'}(z') \mathrm{d}z'. \tag{S24}$$

To do so, consider the integral

$$I = C' \int_0^\infty s^\alpha \hat{\rho}_{z'}^{(n)}(s) \mathrm{d}s = C' \int_0^\infty s^\alpha \int_0^\infty (-1)^n z'^n \rho_{z'}(z') e^{-sz'} \mathrm{d}z' \mathrm{d}s. \tag{S25}$$

Taking into account that for $\alpha > -1$

$$\int_0^\infty s^\alpha e^{-sz'} \mathrm{d}s = z'^{-1-\alpha}\Gamma(1+\alpha), \tag{S26}$$

we see that

$$I = C'(-1)^n\Gamma(1+\alpha)\int_0^\infty z'^{n-1-\alpha}\rho_{z'}(z')\mathrm{d}z'. \tag{S27}$$

Now, setting $C' = (-1)^n\Gamma(1+\alpha)^{-1}$ and $n-1-\alpha = 1/\beta$, $I = \langle z'^{1/\beta}\rangle$. However, since $\alpha = n-1-1/\beta > -1$ and $n \in \mathbb{N}$, the smallest n we can choose is $n = 1$, so $\alpha = -1/\beta$. Finally, we can write

$$\langle\kappa'\rangle = -\frac{1}{\Gamma\left(1-\frac{1}{\beta}\right)}\int_0^\infty s^{-1/\beta}\hat{\rho}'_{z'}(s)\mathrm{d}s, \tag{S28}$$

where $\hat{\rho}_{z'}(s)$ is given in Eq. (S23).

Particular case $r = 2$

To start solving Eq. (S28), let us first take the limit of $N \to \infty \Rightarrow \kappa_c \to \infty$, which means that $\hat{\rho}_z(s)$ becomes

$$\hat{\rho}_z(s) = Cs^{\eta-1}\Gamma(1-\eta, s\kappa_0^\beta), \quad C = \frac{\gamma-1}{\beta\kappa_0^{1-\gamma}}. \tag{S29}$$

Using the same change of variable as in Eq. (S21), we see that

$$\hat{\rho}'_z(s) = -\int_{\kappa_0^\beta}^{\kappa_c^\beta} z\rho_z(z)e^{-sz}\mathrm{d}z = -Cs^{\eta-2}\Gamma(2-\eta, s\kappa_0^\beta). \tag{S30}$$

Let us now evaluate $\hat{\rho}'_{z'}(s)$,

$$\hat{\rho}'_{z'}(s) = r\hat{\rho}_z^{r-1}(s)\hat{\rho}'_z(s) = 2\hat{\rho}_z(s)\hat{\rho}'_z(s) = -2C^2s^{2\eta-3}\Gamma(1-\eta, s\kappa_0^\beta)\Gamma(2-\eta, s\kappa_0^\beta) \tag{S31}$$

and introduce this result into Eq. (S28),

$$\begin{aligned}
\langle\kappa'\rangle &= \frac{2C^2}{\Gamma\left(1-\frac{1}{\beta}\right)}\int_0^\infty s^{2\eta-3-1/\beta}\Gamma(1-\eta, s\kappa_0^\beta)\Gamma(2-\eta, s\kappa_0^\beta)\mathrm{d}s \\
&= \frac{2C^2}{\Gamma\left(1-\frac{1}{\beta}\right)}\frac{1}{\kappa_0^{\beta(2\eta-2-1/\beta)}}\int_0^\infty \omega^{2\eta-3-1/\beta}\Gamma(1-\eta,\omega)\Gamma(2-\eta,\omega)\mathrm{d}\omega \\
&= \kappa_0\frac{2(\gamma-1)^2}{\beta^2\Gamma\left(1-\frac{1}{\beta}\right)}\int_0^\infty \omega^{2\eta-3-1/\beta}\Gamma(1-\eta,\omega)\Gamma(2-\eta,\omega)\mathrm{d}\omega.
\end{aligned} \tag{S32}$$

We thus need to solve an integral of the form

$$I(\nu, s_1, s_2) = \int_0^\infty x^\nu\Gamma(s_1, x)\Gamma(s_2, x)\mathrm{d}x, \quad \nu > -1. \tag{S33}$$

In our case, $\nu = 2\eta - 3 - 1/\beta = (2\gamma-3)/\beta - 1 > -1 \Leftrightarrow \gamma > 3/2$. Integrating by parts,

$$\begin{aligned} I(\nu, s_1, s_2) &= \frac{1}{\nu+1} x^{\nu+1}\Gamma(s_1,x)\Gamma(s_2,x)\Big|_0^\infty + \frac{1}{\nu+1}\int_0^\infty x^{\nu+1}\left(\Gamma(s_1,x)x^{s_2-1}e^{-x} + \Gamma(s_2,x)x^{s_1-1}e^{-x}\right)\mathrm{d}x \\ &= \frac{1}{\nu+1}\int_0^\infty \left(\Gamma(s_1,x)x^{\nu+s_2}e^{-x} + \Gamma(s_2,x)x^{\nu+s_1}e^{-x}\right)\mathrm{d}x. \end{aligned} \tag{S34}$$

We can find a recurrence relation for the integrals in the last expression,

$$\begin{aligned} I'(\alpha, s) &= \int_0^\infty \Gamma(s,x)x^\alpha e^{-x}\mathrm{d}x = \frac{1}{\alpha+1}x^{\alpha+1}\Gamma(s,x)\Big|_0^\infty + \frac{1}{\alpha+1}\int_0^\infty x^{\alpha+1}\left(x^{s-1}e^{-2x} + \Gamma(s,x)e^{-x}\right)\mathrm{d}x \\ &= \frac{1}{\alpha+1}\frac{1}{2^{\alpha+s+1}}\Gamma(\alpha+s+1,2x)\Big|_0^\infty + \frac{1}{\alpha+1}\int_0^\infty \Gamma(s,x)x^{\alpha+1}e^{-x}\mathrm{d}x \\ &= \frac{1}{\alpha+1}\frac{1}{2^{\alpha+s+1}}\Gamma(\alpha+s+1) + \frac{1}{\alpha+1}I'(\alpha+1,s). \end{aligned} \tag{S35}$$

Iterating yields

$$I'(\alpha,s) = \sum_{n=1}^\infty \frac{1}{\prod_{n'=1}^{n}(\alpha+n')}\frac{1}{2^{\alpha+s+n}}\Gamma(\alpha+s+n) = \sum_{n=1}^\infty \frac{\Gamma(\alpha+1)\Gamma(\alpha+s+n)}{\Gamma(\alpha+n+1)2^{\alpha+s+n}}. \tag{S36}$$

Introducing this result into Eq. (S34),

$$\begin{aligned} I(\nu,s_1,s_2) &= \frac{1}{\nu+1}\left(I'(\nu+s_2,s_1) + I'(\nu+s_1,s_2)\right) \\ &= \frac{1}{\nu+1}\sum_{n=1}^\infty\left(\frac{\Gamma(\nu+s_2+1)\Gamma(\nu+s_1+s_2+n)}{\Gamma(\nu+s_2+n+1)2^{\nu+s_1+s_2+n}} + \frac{\Gamma(\nu+s_1+1)\Gamma(\nu+s_1+s_2+n)}{\Gamma(\nu+s_1+n+1)2^{\nu+s_1+s_2+n}}\right) \\ &= \frac{1}{(\nu+1)2^{\nu+s_1+s_2}}\sum_{n=1}^\infty \frac{\Gamma(\nu+s_1+s_2+n)}{2^n}\left(\frac{\Gamma(\nu+s_2+1)}{\Gamma(\nu+s_2+n+1)} + \frac{\Gamma(\nu+s_1+1)}{\Gamma(\nu+s_1+n+1)}\right). \end{aligned} \tag{S37}$$

Finally, Eq. (S32) becomes

$$\begin{aligned} \langle\kappa'\rangle &= \kappa_0\frac{2(\gamma-1)^2}{\beta^2\Gamma\left(1-\frac{1}{\beta}\right)}\int_0^\infty \omega^{2\eta-3-1/\beta}\Gamma(1-\eta,\omega)\Gamma(2-\eta,\omega)\mathrm{d}\omega \\ &= \kappa_0\frac{2(\gamma-1)^2}{\beta^2\Gamma\left(1-\frac{1}{\beta}\right)}I(2\eta-3-1/\beta, 1-\eta, 2-\eta) \\ &= \frac{2^{1+\frac{1}{\beta}}(\gamma-1)^2\kappa_0}{\beta\Gamma\left(1-\frac{1}{\beta}\right)(2\gamma-3)}\sum_{n=1}^\infty \frac{\Gamma\left(n-\frac{1}{\beta}\right)}{2^n}\left(\frac{\Gamma\left(\frac{\gamma-2}{\beta}+1\right)}{\Gamma\left(\frac{\gamma-2}{\beta}+n+1\right)} + \frac{\Gamma\left(\frac{\gamma-2}{\beta}\right)}{\Gamma\left(\frac{\gamma-2}{\beta}+n\right)}\right). \end{aligned} \tag{S38}$$

Using this result, Eq. (S17) and $\kappa_0 = \langle\kappa\rangle(\gamma-2)/(\gamma-1)$ we can write an expression for the exponent ν (defined in the paper by the expression $\langle k'\rangle = r^\nu\langle k\rangle$):

$$\nu = \frac{2}{\ln 2}\ln\left[\frac{2^{1+\frac{1}{\beta}}(\gamma-1)(\gamma-2)}{\beta\Gamma\left(1-\frac{1}{\beta}\right)(2\gamma-3)}\sum_{n=1}^\infty \frac{\Gamma\left(n-\frac{1}{\beta}\right)}{2^n}\left(\frac{\Gamma\left(\frac{\gamma-2}{\beta}+1\right)}{\Gamma\left(\frac{\gamma-2}{\beta}+n+1\right)} + \frac{\Gamma\left(\frac{\gamma-2}{\beta}\right)}{\Gamma\left(\frac{\gamma-2}{\beta}+n\right)}\right)\right] - 1. \tag{S39}$$

The above result is shown in Fig. S4.

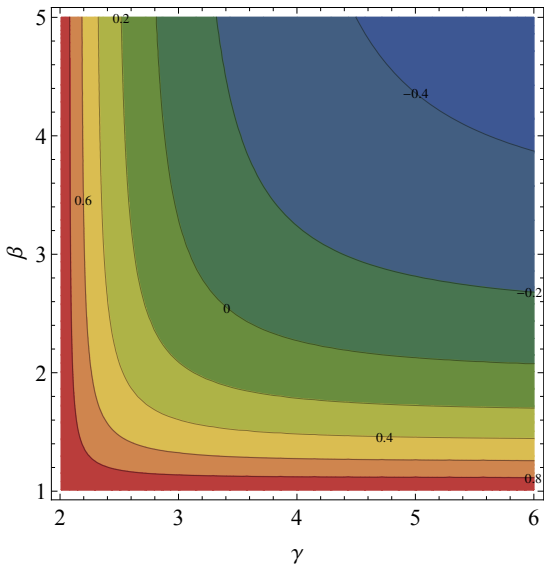

FIG. S4: **Connectivity phase diagram.** Exact value of ν as a function of β and γ according to Eq. (S39). The exact solution agrees with the solution in the power-law approximation (see next subsection) for large values of β or γ.

Solution in the power-law approximation

From Eq. (S38), we see that the exact solution for large r can be extremely convoluted, thus making the limit $r \to \infty$ inaccessible. However, if we consider that $\rho_{\kappa'}(\kappa')$ is a power-law (which is a reasonable approximation if $\eta < 3$, as discussed above), the computation of $\langle \kappa' \rangle$ becomes simpler. Under this assumption, z' are also power-law distributed with exponent $-\eta$, that is,

$$\rho_{z'}(z') = C' z'^{-\eta}, \quad C' = \frac{\gamma - 1}{\beta \kappa_0'^{1-\gamma}}. \tag{S40}$$

We study two cases separately:

i. $1 < \eta < 2$: In this case, we determine the value of C' and, with it, $\langle \kappa' \rangle = \kappa_0' \frac{\gamma-1}{\gamma-2}$. If the assumption in Eq. (S40) is correct, $\hat{\rho}_{z'}(s)$ must behave as [14]

$$\hat{\rho}_{z'}(s) = 1 + C' s^{\eta-1} \Gamma(1-\eta), \quad s \to 0^+. \tag{S41}$$

According to Eqs. (S23) and (S29),

$$\begin{aligned} \hat{\rho}_{z'}(s) = \left[C s^{\eta-1} \Gamma\left(1-\eta, s z_0\right) \right]^r &= \left[C s^{\eta-1} \Gamma\left(1-\eta\right) \left(1 - (s z_0)^{1-\eta} e^{-s z_0} \sum_{n=0}^{\infty} \frac{(s z_0)^n}{\Gamma(2-\eta+n)} \right) \right]^r \\ &= \left[C \Gamma\left(1-\eta\right) \left(s^{\eta-1} - z_0^{1-\eta} e^{-s z_0} \sum_{n=0}^{\infty} \frac{(s z_0)^n}{\Gamma(2-\eta+n)} \right) \right]^r \\ &\to \left[C \Gamma\left(1-\eta\right) \left(s^{\eta-1} - z_0^{1-\eta} \sum_{n=0}^{\infty} \frac{(s z_0)^n}{\Gamma(2-\eta+n)} \right) \right]^r, \quad s \to 0^+. \end{aligned} \tag{S42}$$

In the above expression, we see that the term that does not depend on s is given by the product of the r terms with $n = 0$, whereas the term of order $s^{\eta-1}$ is given by the sum of the r products of $s^{\eta-1}$ with the remaining

$r-1$ terms with $n=0$. Thus, we find

$$\begin{aligned}\hat{\rho}_{z'}(s) &= \left[C\Gamma\left(1-\eta\right)\left(s^{\eta-1}-z_0^{1-\eta}\sum_{n=0}^{\infty}\frac{(sz_0)^n}{\Gamma(2-\eta+n)}\right)\right]^r \\ &\to C^r\Gamma^r\left(1-\eta\right)\left[(-1)^r\frac{z_0^{r(1-\eta)}}{\Gamma^r(2-\eta)}+r(-1)^{r-1}s^{\eta-1}\frac{z_0^{(r-1)(1-\eta)}}{\Gamma^{r-1}(2-\eta)}\right] \\ &= \left(\frac{\gamma-1}{\beta\kappa_0^{1-\gamma}}\right)^r\Gamma^r\left(1-\eta\right)\left[(-1)^r\frac{z_0^{r(1-\eta)}}{(1-\eta)^r\Gamma^r(1-\eta)}+r(-1)^{r-1}s^{\eta-1}\frac{z_0^{(r-1)(1-\eta)}}{(1-\eta)^{r-1}\Gamma^{r-1}(1-\eta)}\right] \\ &= \left(\frac{\eta-1}{z_0^{1-\eta}}\right)^r\left[\frac{z_0^{r(1-\eta)}}{(\eta-1)^r}+rs^{\eta-1}\Gamma\left(1-\eta\right)\frac{z_0^{(r-1)(1-\eta)}}{(\eta-1)^{r-1}}\right] \\ &= 1+r\frac{\eta-1}{z_0^{1-\eta}}s^{\eta-1}\Gamma\left(1-\eta\right).\end{aligned} \tag{S43}$$

We can now identify C' as

$$C'=\frac{\gamma-1}{\beta\kappa_0'^{1-\gamma}}=r\frac{\eta-1}{z_0^{1-\eta}}=r\frac{\gamma-1}{\beta\kappa_0^{1-\gamma}}, \tag{S44}$$

so

$$\kappa_0'=r^{\frac{1}{\gamma-1}}\kappa_0 \tag{S45}$$

and

$$\langle\kappa'\rangle=r^{\frac{1}{\gamma-1}}\langle\kappa\rangle. \tag{S46}$$

Finally, plugging this result into Eq. (S17),

$$\langle k'\rangle=C_0\frac{\mu}{r}r^{\frac{2}{\gamma-1}}\langle\kappa\rangle^2=r^{\frac{2}{\gamma-1}-1}\langle k\rangle\to\begin{cases}\infty & \gamma<3\\ cte. & \gamma=3\\ 0 & \gamma>3\end{cases} \tag{S47}$$

ii. $2<\eta<3$: This case is much simpler, since $\langle z\rangle$ and hence $\langle z'\rangle$ are finite and can be easily computed. Indeed, given that $\langle z'\rangle=r\langle z\rangle$, we see that

$$\begin{aligned}\langle\kappa'\rangle &= \frac{\gamma-1}{\gamma-2}\kappa_0'=\frac{\gamma-1}{\gamma-2}\left(z_0'\right)^{1/\beta}=\frac{\gamma-1}{\gamma-2}\left(\frac{\eta-2}{\eta-1}\langle z'\rangle\right)^{1/\beta}=\frac{\gamma-1}{\gamma-2}\left(\frac{\eta-2}{\eta-1}r\langle z\rangle\right)^{1/\beta} \\ &= \frac{\gamma-1}{\gamma-2}\left(r\frac{\eta-2}{\eta-1}\frac{\eta-1}{\eta-2}z_0\right)^{1/\beta}=\frac{\gamma-1}{\gamma-2}\left(r\kappa_0^{\beta}\right)^{1/\beta}=r^{1/\beta}\langle\kappa\rangle.\end{aligned} \tag{S48}$$

This result and Eq. (S17) together imply

$$\langle k'\rangle=C_0\frac{\mu}{r}r^{2/\beta}\langle\kappa\rangle^2=r^{2/\beta-1}\langle k\rangle\to\begin{cases}\infty & \beta<2\\ cte. & \beta=2\\ 0 & \beta>2\end{cases} \tag{S49}$$

Both solutions, Eqs. (S47) and (S49), are equivalent at $\eta=2$, since

$$\eta=2\Rightarrow\frac{\gamma-1}{\beta}=1\Rightarrow\beta=\gamma-1. \tag{S50}$$

Therefore, we can conclude that the network flows towards a fully connected graph if $\gamma<3$ or $\beta<2$. The line $\gamma=3$ and $\beta>2$ or $\beta=2$ and $\gamma>3$ is formed by unstable fixed points, whereas $\langle k\rangle\to 0$ if $\gamma>3$ and $\beta>2$. Notice that this assertion is only valid under the assumption in Eq. (S40), which is not true in general. However, we expect it to be a good approximation of the flow's behaviour as $r\to\infty$.

E. Renormalization in D-dimensional similarity space

In this subsection, we detail the RG transformations in the general case of a D-dimensional space, as well as the effect of the dimensionality of similarity space on the topology of the resulting networks and the distortion of one-dimensional embeddings.

1. *Model, transformations and average degree flow*

As shown in [15], the connection probability Eq. (S5) in D dimensions reads

$$p_{ij} = \frac{1}{1+\left(\frac{R\Delta\theta_{ij}}{(\mu\kappa_i\kappa_j)^{1/D}}\right)^{\beta}}, \tag{S51}$$

where $\Delta\theta_{ij}$ is the angular separation between the two positioning vectors associated to the nodes embedded in the D dimensional sphere of radius R. Notice that the $1/D$ exponent ensures the proportionality between degrees and hidden degrees. Consequently, Eq. (S11) becomes

$$\left(\frac{R\Delta\theta}{\mu^{1/D}}\right)^{\beta} \frac{1}{\sum\limits_{e=1}^{r^2}(\kappa_m\kappa_n)_e^{\beta/D}} = \left(\frac{R'\Delta\theta'_{ij}}{\left(\mu'\kappa'_i\kappa'_j\right)^{1/D}}\right)^{\beta'}. \tag{S52}$$

Following the same reasoning as in the one-dimensional case, $\beta' = \beta$. Furthermore, we should also require the density of nodes to be preserved, which means that $R' = R/r^{1/D}$. Hence, setting $\mu' = \mu/r$ yields

$$\frac{R'\Delta\theta'}{\mu'^{1/D}} = \frac{R/r^{1/D}\Delta\theta}{(\mu/r)^{1/D}} = \frac{R\Delta\theta}{\mu^{1/D}}, \tag{S53}$$

so the transformation further requires

$$\left(\kappa'_i\kappa'_j\right)^{\beta/D} = \sum_{e=1}^{r^2}(\kappa_m\kappa_n)_e^{\beta/D}, \tag{S54}$$

which is fulfilled by Eqs. (S13) and (S15) with the change $\beta \to \beta/D$. Thus, the analysis of the RG flow of the average degree can be easily generalized by replacing β with β/D in all k'-related quantities.

In the γ-dominated region (now $\beta > D(\gamma-1)$), $\langle\kappa'\rangle$ does not depend on β, so Eq. (S46) still holds and the average degree of the renormalized network is

$$\langle k'\rangle = C_0\frac{\mu}{r}r^{\frac{2}{\gamma-1}}\langle\kappa\rangle^2 = r^{\frac{2}{\gamma-1}-1}\langle k\rangle \to \begin{cases} \infty & \gamma < 3 \\ cte. & \gamma = 3 \\ 0 & \gamma > 3 \end{cases} \tag{S55}$$

In the β-dominated region, on the other hand, $\langle\kappa'\rangle$ becomes $\langle\kappa'\rangle = \langle\kappa\rangle r^{D/\beta}$, so

$$\langle k'\rangle = C_0\frac{\mu}{r}r^{2D/\beta}\langle\kappa\rangle^2 = r^{\frac{2D}{\beta}-1}\langle k\rangle \to \begin{cases} \infty & \beta < 2D \\ cte. & \beta = 2D \\ 0 & \beta > 2D \end{cases} \tag{S56}$$

Both exponents are equal at $\eta = 2$, that is, at $\beta = D(\gamma-1)$. Finally, the non-symmetric phase III, in which $\eta > 3$, corresponds to $\beta < \frac{1}{2}D(\gamma-1)$.

These results show that the dimension of similarity space does not alter the phase diagram qualitatively, but only quantitatively. However, it is interesting to mention that, as the dimension D increases, the small-world phase occupies a region with higher β networks. Moreover, the non-symmetric phase can be found for increasingly heterogeneous networks, that is, for smaller values of γ, at any given value of β.

2. *The dimension of similarity space in real-world networks*

Since the model can be considered in any dimension, it seems reasonable to ask whether a one-dimensional similarity-space representation of real-world networks, for which similarity space could be in general higher-dimensional, suffices. To answer this question, we address two points: firstly, the high clustering coefficient observed in networks poses an upper limit on the similarity-space dimension. Secondly, for low-dimensional similarity-space networks, the one-dimensional embedding provides a faithful representation. We explore these two points in detail in what follows.

As the dimension of a D-sphere increases, the distances between points randomly scattered on its surface become more homogeneous, as shown in Fig. S5. Consequently, the distances in the connection probability become a constant, hence making the model degree-dependent only, which yields a zero-clustering behaviour in the thermodynamic limit. To quantify this effect, we have computed the mean local clustering of the model at zero temperature, $\beta = \infty$—for which the clustering is maximal—, as a function of the dimension for different values of γ. As shown in Fig. S6, for a typical clustering level $\bar{c} > 0.5$, the dimension of similarity space can be, *at most*, $D \approx 10$ ($D \approx 4$ for $\gamma = 3$). This is a very important result, as it suggests that, since the original similarity-space dimension must be low in real-world cases, the distortion introduced by the dimensionality reduction in the one-dimensional similarity-space embedding process might be small.

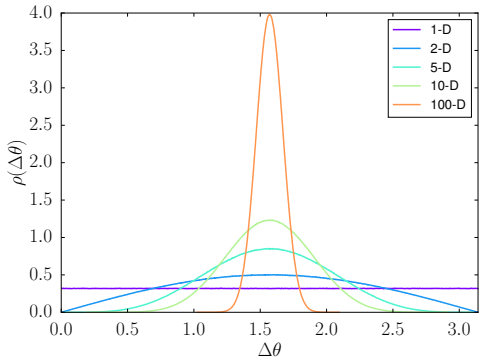

FIG. S5: **Distances on D-spheres.** Every curve corresponds to the distribution of arc-length distances between $N = 10^4$ randomly-scattered points on a D-dimensional sphere. As the dimension increases, the distances become more homogeneously distributed around the mean, $\langle \Delta\theta \rangle = \pi/2$, hence decreasing the clustering in the model.

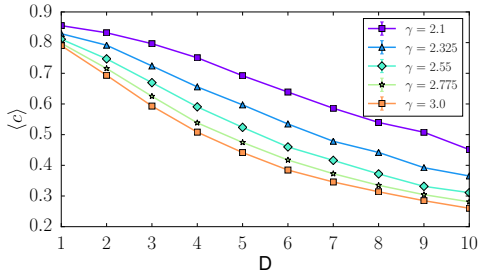

FIG. S6: **Clustering coefficient as a function of the dimension and γ.** The average clustering corresponds to the mean local clustering averaged over 100 realizations on networks of size $N = 1000$; the errorbars, which are smaller than symbol sizes, represent the standard error of the measurement. The value of μ was adjusted so that the observed average degree was $\langle k \rangle = 10.0 \pm 0.1$ in all networks.

In order to assess the possible effect of the dimensionality reduction, we have generated four networks using the $\mathbb{S}^D$ model with the same average degree and clustering coefficient but dimensions $D = 1$, $D = 2$, $D = 5$ and $D = 10$. As Fig. S7 shows, their topologies are extremely similar. Next, we embedded these networks on the $\mathbb{S}^1$ model and measured the quality of the mapping by comparing the original connection probabilities and hyperbolic distances to their counterparts obtained from the embedding (see Fig. S8); although there is some distortion due to the projection onto a lower-dimensional space, the effect on the connection probabilities is mild. Consequently, the one-dimensional embedding is able to recover most of the original geometric information. This is further supported by the fact that

the renormalization procedure yields almost indistinguishable flows when applied to all four networks, as shown in Fig. S9, where the RGN is performed using the embedding distances only.

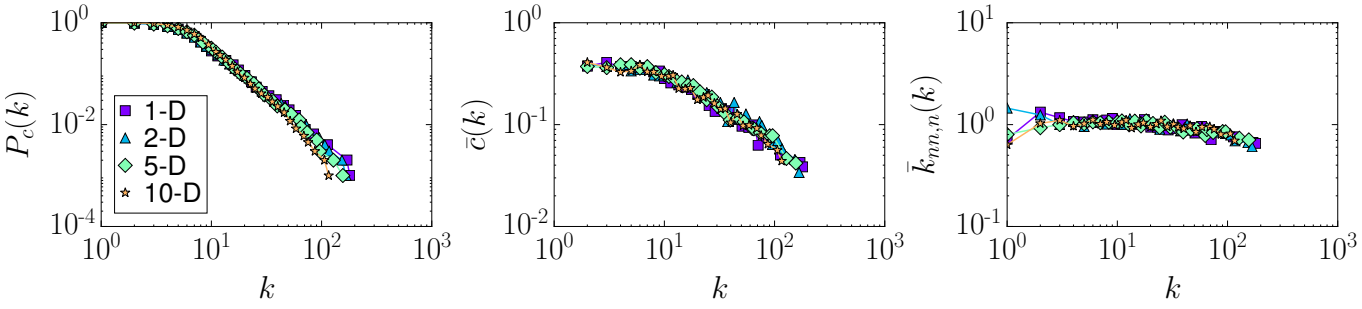

FIG. S7: **Single realizations of the $\mathbb{S}^D$ model.** Topological properties of networks generated with the model in different dimensions. All four networks share the same hidden-degree sequence, while the global parameters μ and β have been adjusted so that they all have the same average degrees and clustering coefficients. **Left:** Complementary cumulative degree distributions. **Middle:** Degree-dependent clustering spectra. **Right:** Normalized average nearest neighbours degrees.

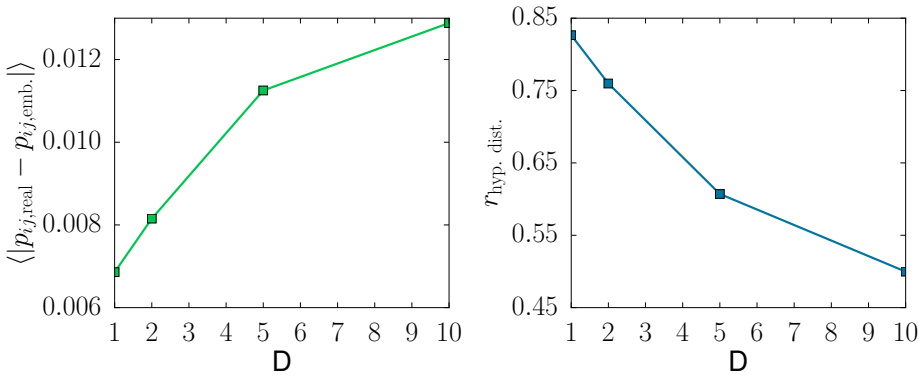

FIG. S8: **Effects of dimensionality reduction. Left:** Absolute differences between the real connection probabilities $p_{ij,\mathrm{real}}$, that is, the ones with which the networks were generated, and the embedding connection probabilities $p_{ij,\mathrm{emb.}}$ averaged over all pairs of nodes. **Right:** Pearson correlation coefficient between the corresponding hyperbolic distances. Notice that, even in the case of original dimension $D = 1$, the embedding process introduces some distortion to the obtained distances and probabilities. For higher dimensions, the effect of the actual geometric distortion is added; yet, the average error in the connection probabilities remains small.

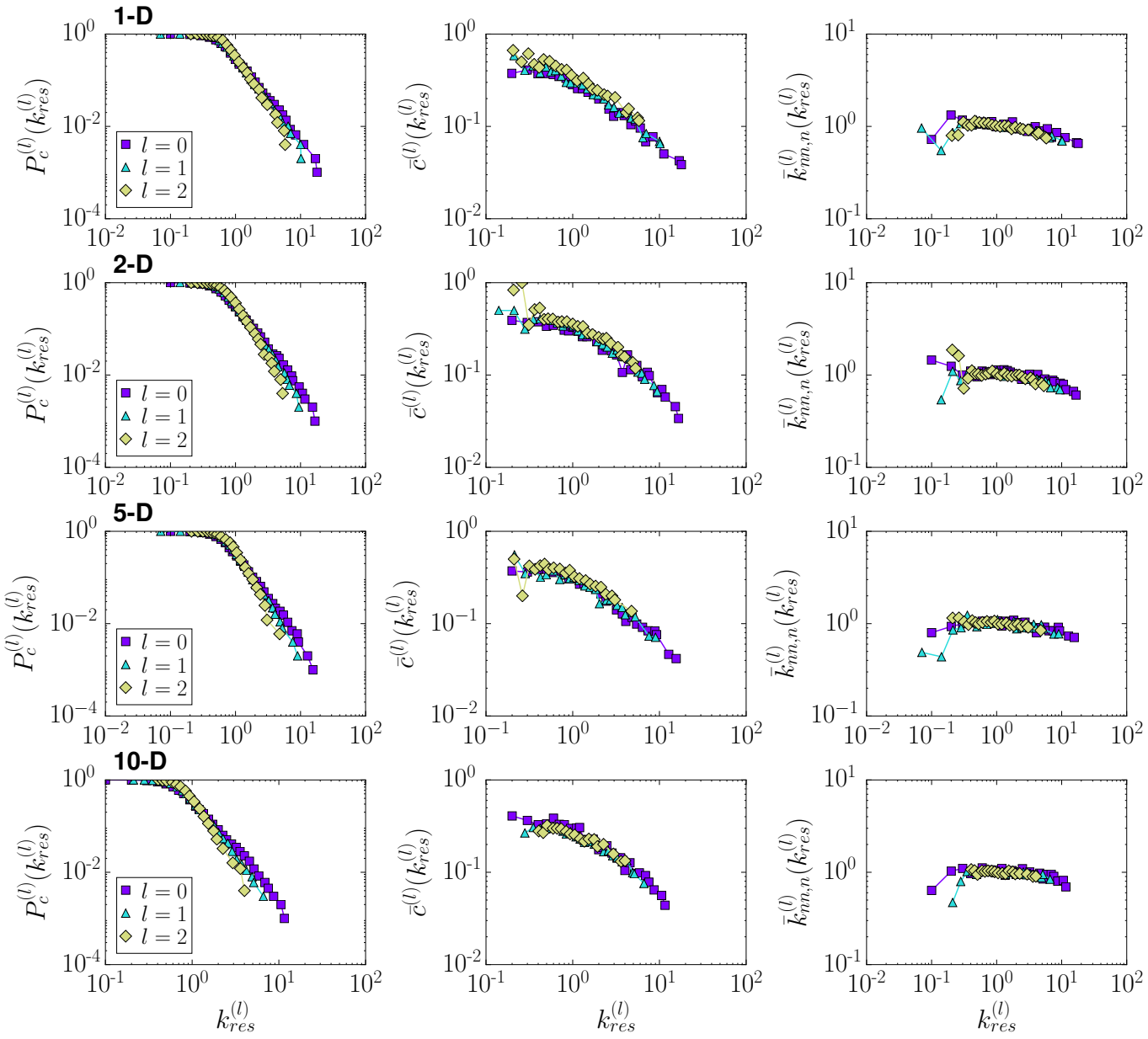

FIG. S9: **RGN flow of topological properties.** Each row shows the RGN flows of the topological features of the networks of different dimensions from Fig. S7. For the transformations, only information from the one-dimensional embedding was used. **Left:** Complementary cumulative distribution of rescaled degrees $k_{res}^{(l)} = k^{(l)}/\langle k^{(l)}\rangle$. **Middle:** Local clustering averaged over rescaled-degree classes. **Right:** Normalized average nearest neighbour degree $\bar{k}_{nn,n}(k_{res}^{(l)}) = \bar{k}_{nn}(k_{res}^{(l)})\langle k^{(l)}\rangle/\langle (k^{(l)})^2\rangle$.

F. Mapping to hyperbolic space and the partition function

In this section, we show how the RGN presented in this work can be described in the formalism of statistical physics. The $\mathbb{S}^1$ model is isomorphic to the $\mathbb{H}^2$ model, a purely geometric model in a two-dimensional hyperbolic disk of radius

$$R_{\mathbb{H}^2} = 2\ln\left(\frac{2R}{\mu\kappa_0^2}\right), \tag{S57}$$

where $\kappa_0 = \min\{\kappa_i\}$. By mapping every mass κ to a radial coordinate r according to

$$r = R_{\mathbb{H}^2} - 2\ln\frac{\kappa}{\kappa_0}, \tag{S58}$$

the connection probability, Eq. (S5), becomes

$$p_{mn} = \frac{1}{1+e^{\frac{\beta}{2}(x_{mn}-R_{\mathbb{H}^2})}}, \tag{S59}$$

where $x_{mn} = r_m + r_n + 2\ln\frac{\Delta\theta_{mn}}{2}$ is a good approximation to the hyperbolic distance between two points with coordinates (r_m,θ_m) and (r_n,θ_n) in the native representation of hyperbolic space. The exact hyperbolic distance $d_{\mathbb{H}^2}$ is given by the hyperbolic law of cosines,

$$d_{\mathbb{H}^2} = \operatorname{acosh}\left(\cosh r_m \cosh r_n - \sinh r_m \sinh r_n \cos\Delta\theta_{mn}\right). \tag{S60}$$

Now, let $a_{mn}=1$ if the link between nodes m and n exists and $a_{mn}=0$ otherwise; Eq. (S59) can be written as

$$p_{mn} \equiv P(a_{mn}) = \frac{e^{-\beta\frac{a_{mn}}{2}(x_{mn}-R_{\mathbb{H}^2})}}{1+e^{-\frac{\beta}{2}(x_{mn}-R_{\mathbb{H}^2})}}, \tag{S61}$$

which means that, in the $\mathbb{H}^2$ model, every pair of nodes represents a fermionic state of energy $x_{mn}/2$ in the grand-canonical ensemble with $R_{\mathbb{H}^2}/2$ playing the role of the chemical potential. Indeed, since a network can be represented by the set $\{a_{mn}\}$, the likelihood of a given network is given by

$$P(\{a_{mn}\}) = \prod_{m<n}\frac{e^{-\beta\frac{a_{mn}}{2}(x_{mn}-R_{\mathbb{H}^2})}}{1+e^{-\frac{\beta}{2}(x_{mn}-R_{\mathbb{H}^2})}}, \tag{S62}$$

that is, by the probability of the corresponding microstate of the gas of non-interacting fermions. The partition function of the system is

$$Z = \prod_{m<n}\sum_{a_{mn}=0}^{1} e^{-\beta\frac{a_{mn}}{2}(x_{mn}-R_{\mathbb{H}^2})} = \prod_{m<n}\left(1+e^{-\frac{\beta}{2}(x_{mn}-R_{\mathbb{H}^2})}\right). \tag{S63}$$

When we apply the renormalization transformation, every node m (n) is mapped to a supernode i (j). We can rearrange the terms in the partition function according to such mapping as

$$Z = \prod_{i=1}^{\lfloor\frac{N}{r}\rfloor}\prod_{t=1}^{\frac{r(r-1)}{2}}\left(1+e^{-\frac{\beta}{2}(x_t-R_{\mathbb{H}^2})}\right)\prod_{i<j}\prod_{e=1}^{r^2}\left(1+e^{-\frac{\beta}{2}(x_e-R_{\mathbb{H}^2})}\right). \tag{S64}$$

The first double product in the above expression corresponds to the partial sum over the links among the nodes within every supernode i (hence, there are $N(r-1)/2$ such terms), whereas the second double product represents the partial sum over the links among nodes in different supernodes i and j; thus, it contains $(N^2-Nr)/2$ terms. According to Eqs. (S57) and (S58),

$$e^{-\frac{\beta}{2}(x_{mn}-R_{\mathbb{H}^2})} = \left(\frac{\mu\kappa_m\kappa_n}{R\Delta\theta_{mn}}\right)^{\beta}, \tag{S65}$$

so the rightmost term in Eq. (S64) reads

$$\prod_{i<j}\prod_{e=1}^{r^2}\left(1+e^{-\frac{\beta}{2}(x_e-R_{\mathbb{H}^2})}\right) = \prod_{i<j}\prod_{e=1}^{r^2}\left(1+\left(\frac{\mu(\kappa_m\kappa_n)_e}{R\Delta\theta_e}\right)^{\beta}\right) = \prod_{i<j}\left(1+\Phi'_{ij}\right), \tag{S66}$$

where Φ'_{ij} is given by Eq. (S7). Using Eq. (S9) and Eq. (S11), which is fulfilled with the RG transformations derived in Sect. II C, yields

$$\begin{aligned}\prod_{i<j}\prod_{e=1}^{r^2}\left(1+e^{-\frac{\beta}{2}(x_e-R_{\mathbb{H}^2})}\right) &\approx \prod_{i<j}\left(1+\left(\frac{\mu}{R\Delta\theta}\right)^{\beta}\sum_{e=1}^{r^2}(\kappa_m\kappa_n)_e^{\beta}\right)\\ &= \prod_{i<j}\left(1+\left(\frac{\mu'\kappa'_i\kappa'_j}{R'\Delta\theta'_{ij}}\right)^{\beta}\right) = \prod_{i<j}\left(1+e^{-\frac{\beta}{2}(x'_{ij}-R'_{\mathbb{H}^2})}\right) = Z'.\end{aligned} \tag{S67}$$

The leftmost term in Eq. (S64) can be written as

$$\prod_{i=1}^{\lfloor \frac{N}{r} \rfloor} \prod_{t=1}^{\frac{r(r-1)}{2}} \left(1 + e^{-\frac{\beta}{2}(x_t - R_{\mathbb{H}^2})}\right) = \prod_{i=1}^{\lfloor \frac{N}{r} \rfloor} \prod_{t=1}^{\frac{r(r-1)}{2}} \left(1 + \left(\frac{\mu(\kappa_m \kappa_n)_t}{R\Delta\theta_t}\right)^{\beta}\right). \tag{S68}$$

In the particular case of $r = 2$, we integrate consecutive nodes separated by a typical angular distance $\Delta\theta_t \approx 2\pi/N$. Hence, $R\Delta\theta_t \approx 1$, so

$$\prod_{i=1}^{\lfloor \frac{N}{r} \rfloor} \prod_{t=1}^{\frac{r(r-1)}{2}} \left(1 + e^{-\frac{\beta}{2}(x_t - R_{\mathbb{H}^2})}\right) \approx e^{\sum_{i=1}^{\lfloor N/2 \rfloor} \ln\left(1+(\mu(\kappa_m \kappa_n)_i)^{\beta}\right)} \approx e^{\frac{N}{2}\left\langle \ln\left(1+(\mu\kappa_m\kappa_n)^{\beta}\right)\right\rangle}. \tag{S69}$$

Defining

$$\zeta \equiv e^{\left\langle \ln\left(1+(\mu\kappa_m\kappa_n)^{\beta}\right)\right\rangle} = e^{\int \ln\left(1+(\mu\kappa_m\kappa_n)^{\beta}\right)\rho(\kappa_m)\rho(\kappa_n)d\kappa_m d\kappa_n} \tag{S70}$$

we can write Eq. (S64) as

$$Z = \zeta^{N/2} Z', \tag{S71}$$

where $Z' = \sum_{\{a_{ij}\}} e^{-\beta H'(\{a_{ij}\})}$.

G. Local vs. global properties

In the $\mathbb{S}^1$ model, we impose three parameters, γ, β and $\langle\kappa\rangle$, all three related to local properties of nodes (degree and clustering). However, the RG flow of observables like the average degree should be related to global properties of the system; indeed, we would expect two networks with similar average degree flows to exhibit similarities at the global scale as well, whereas two networks with very different RG trajectories (even in the same phase, i.e., flowing towards the same fixed point) should be easier to distinguish by looking at their global properties. To check this hypothesis, we have generated synthetic networks with different values of γ and β and compared the eigenvalues of both the adjacency and laplacian matrices. The results are shown in Figs. S10, S11 and S12. As we see, the RG analysis of the model allows us to assess the stability of the global properties of networks against perturbations of their local ones, and hence the importance of clustering and degree heterogeneity on a given system.

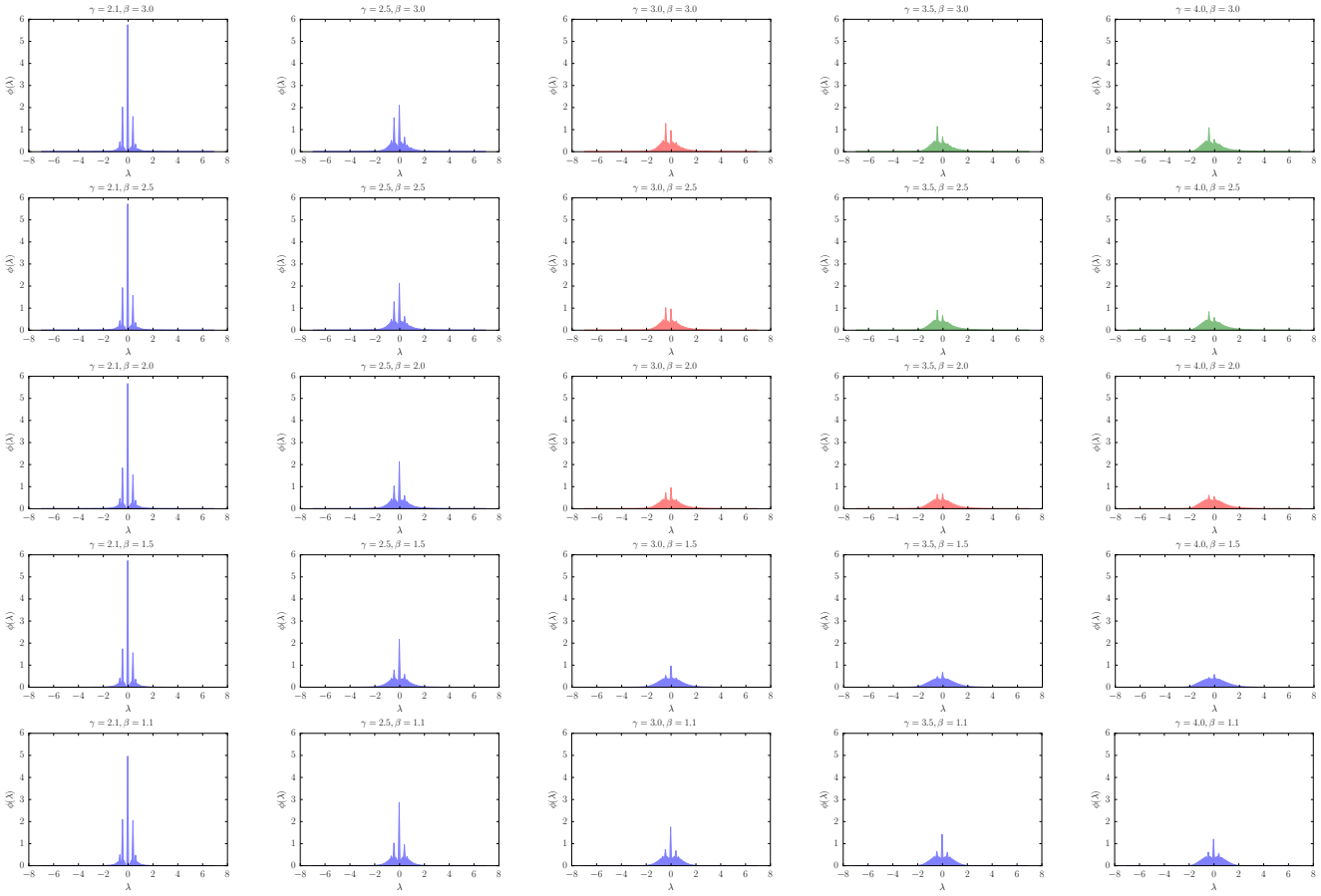

FIG. S10: **Eigenvalues of adjacency matrices.** Every plot represents a histogram of the eigenvalues (divided by $\sqrt{\langle\kappa\rangle}$) of the adjacency matrices of 100 synthetic networks of size $N = 1000$ and $\langle\kappa\rangle = 5$ for a particular set of values (γ, β). The order of the plots corresponds to that of the phase diagram Fig. 3**C** in the paper. Notice how the RG analysis correctly predicts the dependence of the spectra on γ only on the top-left corner of the figure, as well as the independence on γ on the bottom-right region.

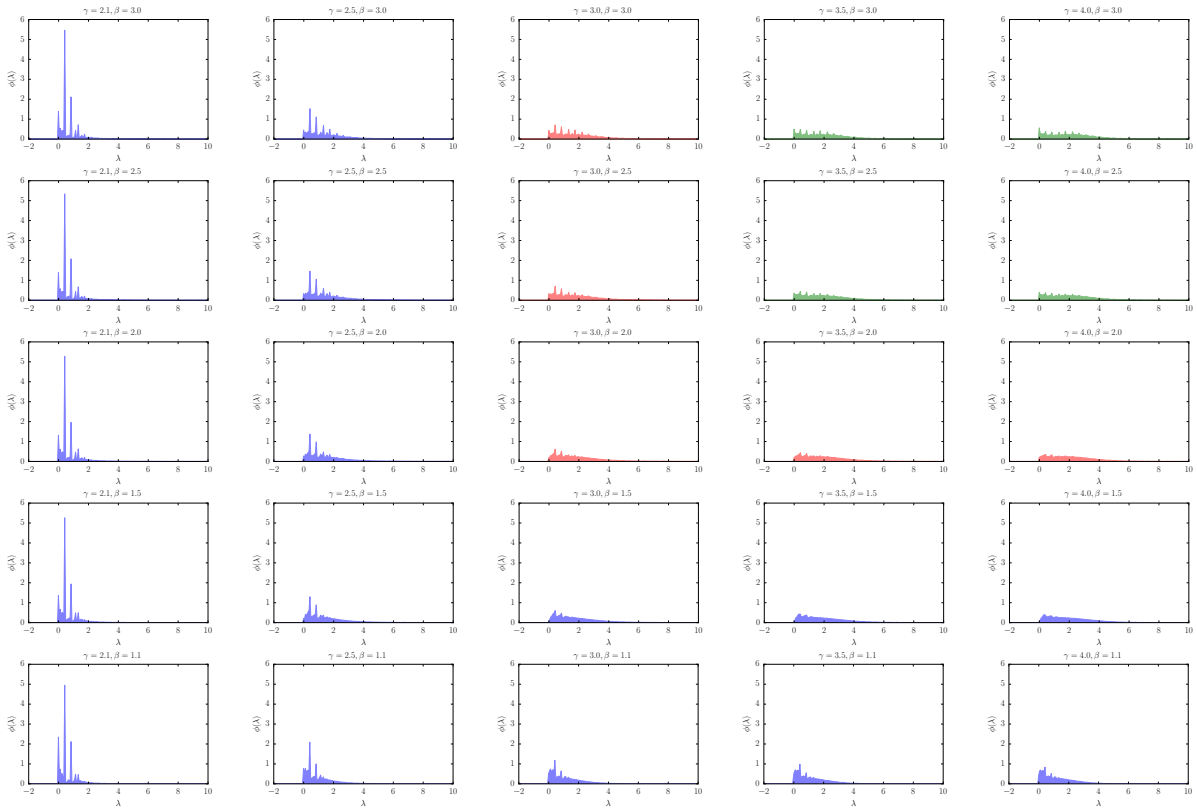

FIG. S11: **Eigenvalues of laplacian matrices.** Every plot represents a histogram of the eigenvalues (divided by $\sqrt{\langle\kappa\rangle}$) of the laplacian matrices of 100 synthetic networks of size $N = 1000$ and $\langle\kappa\rangle = 5$ for a particular set of values (γ, β). The order of the plots corresponds to that of the phase diagram Fig. **3C** in the paper. Notice how the RG analysis correctly predicts the dependence of the spectra on γ only on the top-left corner of the figure, as well as the independence on γ on the bottom-right region.

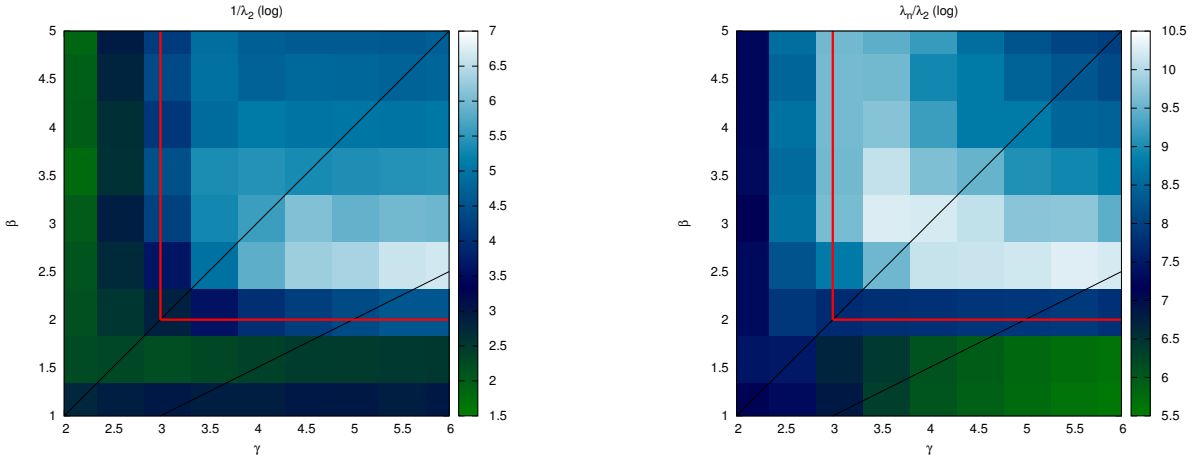

FIG. S12: **Diffusion time and synchronization stability. Left:** Logarithm of the diffusion time (inverse of the algebraic connectivity or first non-null eigenvalue of the laplacian λ_2) of networks of size $N = 1000$ and $\langle\kappa\rangle = 5$ averaged over 100 realizations. **Bottom:** Logarithm of the quotient λ_n/λ_2 (this quantity is related to the stability of synchronization processes on networks; it gives the time that the system needs to get back to the stable synchronized state after a perturbation occurred). In both plots, we can see the similarities with Fig. **3C** in the paper.

III. DOWNSCALED NETWORK REPLICAS

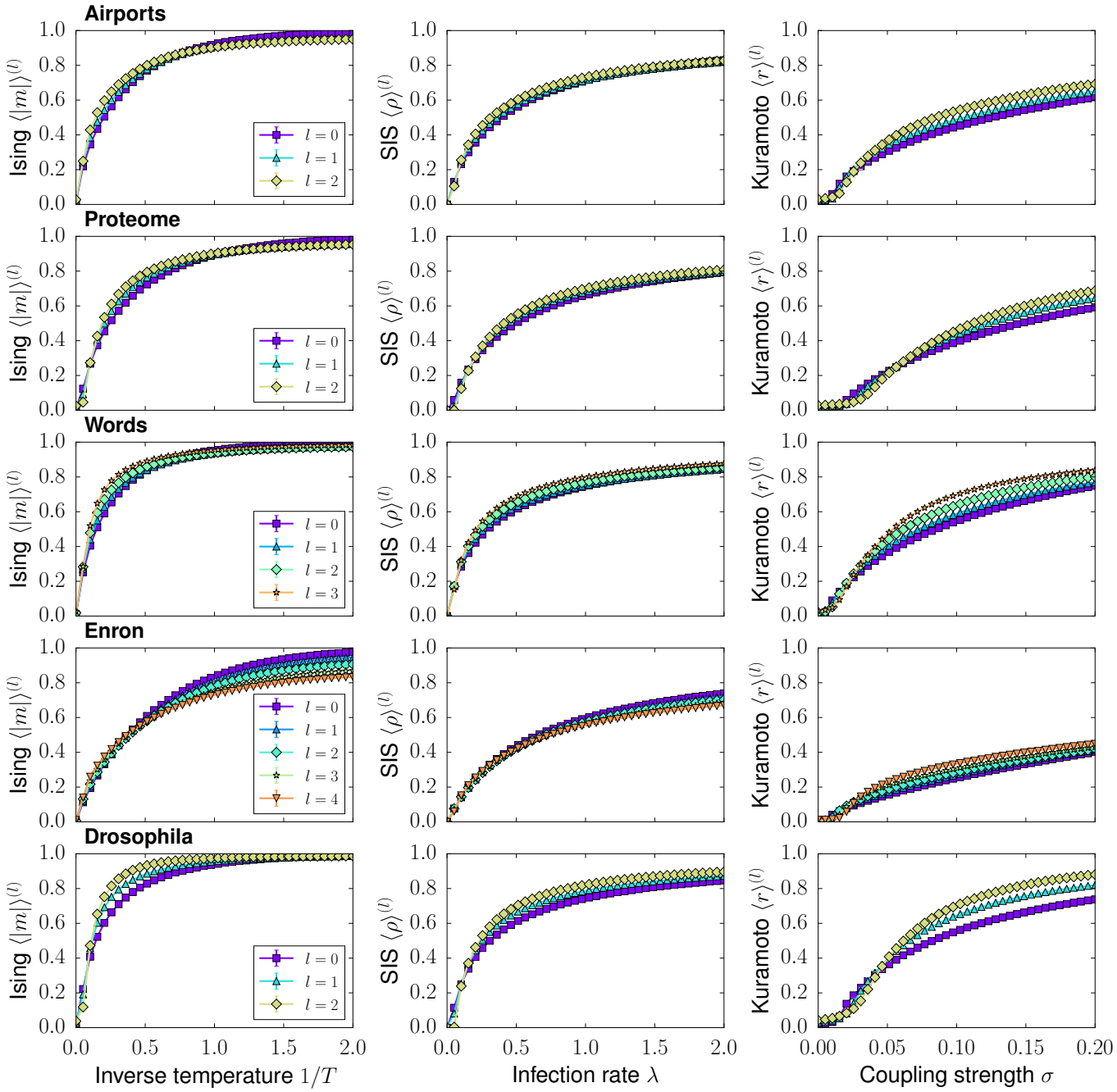

FIG. S13: **Dynamics on the downscaled network replicas.** Each row shows the order parameters versus the control parameters of different dynamical processes on the original and downscaled replicas of the Airports, Proteome, Words, Enron and Drosophila networks with $r = 2$, that is, every value of l identifies a network 2^l times smaller than the original one. All points show the results averaged over 100 simulations. Error bars indicate the standard deviations of the order parameters. **Left:** Magnetization $\langle |m| \rangle^{(l)}$ of the Ising model as a function of the inverse temperature $1/T$. **Middle:** Prevalence $\langle \rho \rangle^{(l)}$ of the SIS model as a function of the infection rate λ. **Right:** Coherence $\langle r \rangle^{(l)}$ of the Kuramoto model as a function of the coupling strength σ. In all cases, the curves of the smaller-scale replicas are extremely similar to the results obtained on the original networks.

IV. MULTISCALE NAVIGATION NETWORKS

This section includes some results showing the topological properties of the coarse-grained for navigation networks; Fig. S14 shows the complementary cumulative degree distributions, whereas Fig. S15 contains their clustering spectra.

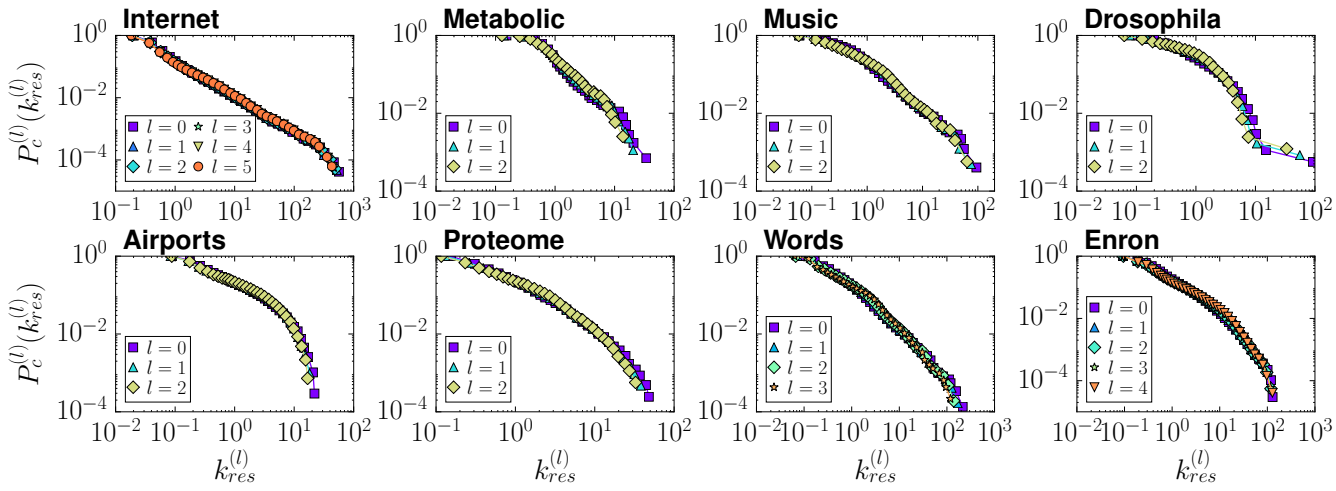

FIG. S14: **Complementary cumulative degree distributions.** Every curve represents the complementary cumulative degree distribution of a given layer in the multiscale navigation shell.

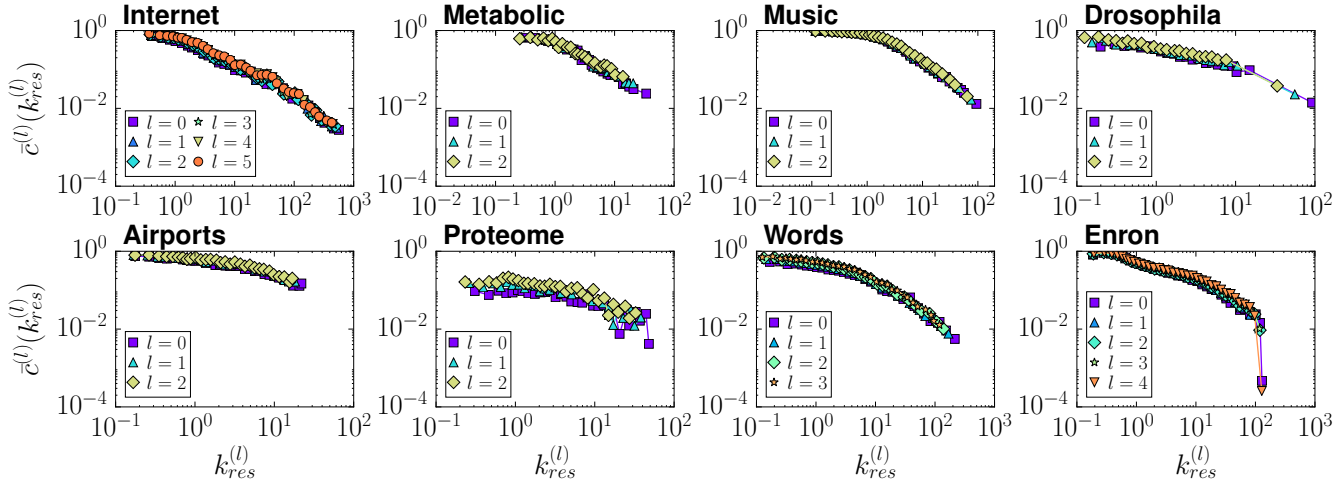

FIG. S15: **Clustering spectra.** Every curve represents the clustering spectrum of a given layer in the multiscale navigation shell.

We also present the empirical connection probabilities of the networks after the coarse-graining for navigation (in which pairs of nodes are merged together into a supernode only if they are connected) in Fig. S16. Notice that the congruency with the underlying metric space is preserved even is the sizes of the blocks are different.

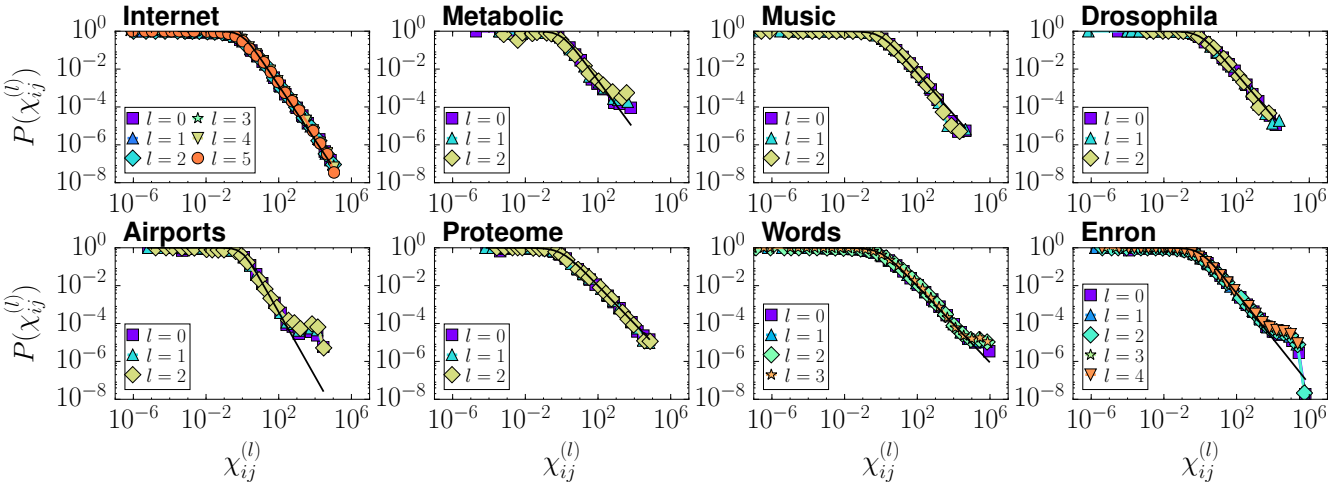

FIG. S16: **Empirical connection probabilities.** Fraction of connected pairs within a given range of $\chi_{ij}^{(l)}$ for the eight real-world networks and their coarse-grained for navigation versions. The black curve is the theoretic connection probability.

[1] K. Claffy, Y. Hyun, K. Keys, M. Fomenkov, and D. Krioukov, in *CATCH* (2009), http://www.caida.org/projects/ark/.

[2] *Openflights network dataset – KONECT* (2016), URL `http://konect.uni-koblenz.de/networks/openflights`.

[3] J. Kunegis, in *Proc. Int. Conf. on World Wide Web Companion* (2013), pp. 1343–1350, URL `http://userpages.uni-koblenz.de/~kunegis/paper/kunegis-koblenz-network-collection.pdf`.

[4] M. A. Serrano, M. Boguna, and F. Sagues, Mol. BioSyst. **8**, 843 (2012).

[5] T. Rolland, M. Taan, B. Charloteaux, S. Pevzner, Q. Zhong, N. Sahni, S. Yi, I. Lemmens, C. Fontanillo, R. Mosca, et al., Cell **159**, 1212 (2014), ISSN 0092-8674, URL `http://www.sciencedirect.com/science/article/pii/S0092867414014226`.

[6] J. Serrà, A. Corral, M. Boguñá, M. Haro, and J. L. Arcos, Scientific Reports **2** (2012), URL `http://www.nature.com/srep/2012/120726/srep00521/full/srep00521.html`.

[7] M. Á. Serrano, M. Boguñá, and A. Vespignani, Proc. Natl. Acad. Sci. USA **106**, 6483 (2009).

[8] R. Milo, S. Itzkovitz, N. Kashtan, R. Levitt, S. Shen-Orr, I. Ayzenshtat, M. Sheffer, and U. Alon, Science **303**, 1538 (2004).

[9] B. Klimt and Y. Yang, in *CEAS* (2004), URL `http://dblp.uni-trier.de/db/conf/ceas/ceas2004.html#KlimtY04`.

[10] J. Leskovec, K. J. Lang, A. Dasgupta, and M. W. Mahoney, Internet Mathematics **6**, 29 (2009), http://dx.doi.org/10.1080/15427951.2009.10129177, URL `http://dx.doi.org/10.1080/15427951.2009.10129177`.

[11] S.-y. Takemura, A. Bharioke, Z. Lu, A. Nern, S. Vitaladevuni, P. K. Rivlin, W. T. Katz, D. J. Olbris, S. M. Plaza, P. Winston, et al., Nature **500**, 175 (2013), ISSN 0028-0836, article, URL `http://dx.doi.org/10.1038/nature12450`.

[12] D. Krioukov, F. Papadopoulos, M. Kitsak, A. Vahdat, and M. Boguñá, Phys Rev E **82**, 036106 (2010).

[13] B. Gnedenko and A. Kolmogorov, *Limit distributions for sums of independent random variables*, Addison-Wesley series in statistics (Addison-Wesley, 1968).

[14] R. A. Handelsman and J. S. Lew, SIAM Journal on Mathematical Analysis **5**, 425 (1974).

[15] A. Allard, M. Á. Serrano, G. García-Pérez, and M. Boguñá, Nature Communications **8**, 14103 (2017), URL `http://dx.doi.org/10.1038/ncomms14103`.